

Locking and regularization of chimeras by periodic forcingMaxim I. Bolotov¹, Lev A. Smirnov^{2,1}, Grigory V. Osipov¹, and Arkady Pikovsky^{3,1,4}¹*Department of Control Theory, Research and Education Mathematical Center “Mathematics for Future Technologies,” Nizhny Novgorod State University, Gagarin Av. 23, 603950, Nizhny Novgorod, Russia*²*Institute of Applied Physics of the Russian Academy of Sciences, Ul’yanov Str. 46, 603950, Nizhny Novgorod, Russia*³*Institute of Physics and Astronomy, University of Potsdam, Karl-Liebknecht-Straße 24-25, 14476 Potsdam, Germany*⁴*National Research University Higher School of Economics, 25/12 Bolshaya Pecherskaya Ulitsa, 603155 Nizhny Novgorod, Russia*

(Received 13 December 2019; revised 6 August 2020; accepted 28 September 2020; published 26 October 2020)

We study how a chimera state in a one-dimensional medium of nonlocally coupled oscillators responds to a homogeneous in space periodic in time external force. On a macroscopic level, where a chimera can be considered as an oscillating object, forcing leads to entrainment of the chimera’s basic frequency inside an Arnold tongue. On a mesoscopic level, where a chimera can be viewed as an inhomogeneous, stationary, or nonstationary pattern, strong forcing can lead to regularization of an unstationary chimera. On a microscopic level of the dynamics of individual oscillators, forcing outside of the Arnold tongue leads to a multiplateau state with nontrivial locking properties.

DOI: [10.1103/PhysRevE.102.042218](https://doi.org/10.1103/PhysRevE.102.042218)**I. INTRODUCTION**

Chimeras in nonlocally coupled oscillator populations are spectacular patterns combining synchronous and asynchronous patches. Since the first observation by Kuramoto and Battogtokh [1], significant progress has been achieved in theoretical and experimental exploration of chimeras; see recent reviews [2,3]. On a microscopic level, the Kuramoto-Battogtokh chimera demonstrates coexistence of ordered and disordered domains: neighboring units are either fully synchronized or partially correlated. On a mesoscopic level, when one introduces a coarse-grained order parameter, a chimera constitutes a nonhomogeneous pattern with a continuous profile of the complex order parameter; the latter has absolute value one in synchronized domains and is less than one in disordered regions. On a macroscopic level, a chimera can be treated as an inhomogeneous oscillating structure.

In a homogeneous medium, because of the invariance to shifts in space and time, a chimera pattern is expected to be sensitive to a weak inhomogeneity in space and to a small time-dependent forcing. The former option was explored in Refs. [4,5], where it was demonstrated that a weak inhomogeneity controls a chimera’s position in space. In this paper we focus on a time-periodic uniform in space forcing. The main guiding point is that the chimera as a whole is an oscillating object, and, thus, similar to simple self-sustained oscillators, it can be phase locked or frequency entrained. In particular, two coupled chimeras can synchronize in the sense of entrainment of their mean frequencies, while the internal inhomogeneous structure of order-disorder is preserved [6,7].

In this paper we explore synchronization properties of chimera patterns subject to a periodic in time and homogeneous in space external force. We employ the reduction approach of Ref. [8] and formulate the problem of finding chimera patterns locked to the external field as a problem of finding periodic orbits in a system of ordinary differential

equations. At this macroscopic level, we determine chimeras with stable and unstable phase shifts to the forcing, and regions of their existence (“Arnold tongues”) on the plane of forcing parameters “amplitude-frequency.” On the mesoscopic level, locked chimeras can be stationary, breathing, or turbulent, and we characterize these states through distributions of the oscillators mean frequencies. Outside the locked region, interesting microscopic patterns appear, where some subgroups of oscillators are mutually entrained, and some of them are entrained by the external force (while the chimera as a whole is not).

We start with formulation of the basic equations in Sec. II. Here we also introduce fundamental properties of chimeras on macroscopic, mesoscopic, and microscopic levels. In Sec. III we describe our method of finding locked chimeras by virtue of reduction to a set of ordinary differential equations. We also briefly discuss here how the stability of these states is determined. Then we describe in Sec. IV different static, periodic, and turbulent chimera states observed under forcing. We conclude with Sec. V. In Appendix A we present the details of the developed numerical chimera-seeking approach. In Appendix B we consider a procedure which allows one to attribute the found uniformly rotating chimeras to specific regions on the plane of forcing parameters “amplitude-frequency” at a given medium length, and consequently to construct synchronization domains for such states. Appendix C contains some key aspects of the linear stability analysis for standing chimera patterns.

II. FORMULATION OF THE PROBLEM**A. Basic equations**

As a basic model we use the Kuramoto-Battogtokh setup [1] with additional periodic forcing. We assume that N oscillators described by their phases φ_n are arranged in a ring

and are nonlocally coupled with a coupling kernel $G_{n,\bar{n}} = LG(L(n - \bar{n})/N)/N$:

$$\frac{d\varphi_n}{dt} = \text{Im} \left(e^{-i(\varphi_n + \alpha)} \sum_{\bar{n}=1}^N G_{n,\bar{n}} e^{i\varphi_{\bar{n}}} + \varepsilon e^{i(\Omega t - \varphi_n)} \right). \quad (1)$$

While this model will be used in numerical examples below, for the theoretical description it is convenient to go to the continuous space limit, treating $x = Ln/N$ as a continuous variable. Here the setup is a one-dimensional oscillatory medium of length L , enclosed in a ring, and described by phases $\varphi(x, t)$, which are coupled nonlocally. This medium is additionally subject to a uniform force with amplitude ε and frequency Ω :

$$\partial_t \varphi = \text{Im} \left[e^{-i(\varphi + \alpha)} \int_0^L G(x - \bar{x}) e^{i\varphi(\bar{x}, t)} d\bar{x} + \varepsilon e^{i(\Omega t - \varphi)} \right]. \quad (2)$$

Here the kernel

$$G(x) = \cosh(|x| - L/2) / 2 \sinh(L/2) \quad (3)$$

is a regularized (for periodic boundary conditions) version of the exponential kernel used by Kuramoto and Battogtokh [1,8]. It is noteworthy that the kernel $G(x)$ defined by expression (3) is the inverse of the operator $(\partial_{xx} - 1)$ in the periodic domain of length L , while the exponential kernel is the inverse in the infinite domain; cf., Eq. (6) below.

The first step in the analysis is the introduction of the coarse-grained order parameter $Z(x, t) = \langle e^{i\varphi(x,t)} \rangle_\delta$ via averaging over a small vicinity δ of point x [8–11]. Physically, the amplitude of this complex function [which satisfies the inequality $|Z(x, t)| \leq 1$] fully describes the level of synchrony of the phases $\varphi(x, t)$ in a small neighborhood of point x . In a region where $|Z(x, t)| = 1$, the neighboring elements move synchronously. When $|Z(x, t)| < 1$, the neighboring phase oscillators rotate asynchronously. The complex order parameter $Z(x, t)$ obeys the Ott-Antonsen equation [8–11]

$$\partial_t Z = (e^{-i\alpha} H - e^{i\alpha} H^* Z^2) / 2, \quad (4)$$

$$H(x, t) = \varepsilon e^{i(\Omega t + \alpha)} + \int_0^L G(x - \bar{x}) Z(\bar{x}, t) d\bar{x}. \quad (5)$$

Here we introduce an auxiliary macroscopic field $H(x, t)$, which describes the driving force on oscillators in a small vicinity of point x . Using a specific form (3) for the kernel $G(x)$, the integral relation (5) between $Z(x, t)$ and $H(x, t)$ can be equivalently written as the following differential equation:

$$\partial_{xx}^2 H - H = -Z - \varepsilon e^{i(\Omega t + \alpha)}. \quad (6)$$

Thus, the problem of finding forced chimera states can be formulated as that of finding nontrivial patterns in the system of partial differential equations (4) and (6). Below we fix $\alpha = 1.457$, the value adopted in Ref. [1].

B. Microscopic, mesoscopic, and macroscopic levels of chimera descriptions

Above we introduced a hierarchy of equations describing a set of coupled oscillators, and correspondingly one can formulate different levels at which the chimera state can be treated. It is instructive to introduce these levels and to outline possible

approaches for their treatment starting from free, nonforced chimeras.

At the *macroscopic* level, one can treat a chimera as a periodic in time (with some frequency Ω_0) solution of macroscopic equations (4) and (5), having a nontrivial spatial structure of the complex order parameter Z . If one looks at this solution as a “limit cycle” in the infinite-dimensional phase space, then one can expect that the effect of a periodic force on a chimera will be similar to the known properties of synchronization of periodic self-sustained oscillators by an external forcing. Namely, there will be a synchronization region (Arnold tongue), where the solution remains basically the same as without forcing, only its frequency will be entrained by the external forcing frequency Ω . Practically, finding a free chimera solution is a nontrivial problem. In Ref. [12] it is formulated as a nonlinear eigenvalue problem, and examples of different macroscopic solutions are given for a piecewise constant and for cosine coupling kernels (where the Galerkin method was adopted to reduce the dimension of the infinite-dimensional problem). The basic chimera state for an exponential kernel has been found as a solution of the nonlinear self-consistency problem in Ref. [1]. In our previous publication [8] we used an alternative approach for the kernel (3). Here the problem reduces to a set of partial differential equations, which for uniformly rotating patterns further reduces to a set of equations containing spatial derivatives only. As a result, the problem of finding uniformly rotating patterns reduces to the problem of finding periodic solutions of a three-dimensional system of ordinary differential equations. This is a much simpler task than that of finding fixed points for a high-dimensional Galerkin approximation of an infinite-dimensional nonlinear eigenvalue problem. Indeed, in this way, many chimera profiles have been found in Ref. [8]. Below we show how this latter approach can be generalized for the forced chimera (potentially, also Galerkin methods for solving the nonlinear eigenvalue problem could be generalized for the driven system).

At the *mesoscopic* level, one takes into account the possibly complex spatiotemporal dynamics of the solution, remaining, however, on the level of coarse-grained description in terms of the order parameter $Z(x, t)$, obeying system (4) and (5). Here, in particular, stability properties of the obtained solutions are essential. One distinguishes here stationary chimeras with a time-independent (in the rotating frame of the basic frequency Ω_0) profile of the order parameter, and turbulent chimeras with periodic pulsations of the order parameter, and turbulent chimeras. The two latter states cannot be interpreted as (high-dimensional) limit cycles, rather they correspond to quasiperiodic and chaotic attractors. Synchronization properties of such systems are nontrivial. We will see that here the locking of the basic chimera frequency (understood as one of the basic frequencies in the quasiperiodic case; and as the mean frequency of the overall order parameter in the turbulent case, this latter situation corresponds to so-called phase synchronization of chaotic oscillators [13]) also can be achieved by an external driving. Furthermore, we will see that inside the corresponding entrainment region (which can also be named an Arnold tongue) stability properties can be governed by the driving: an entrained breathing chimera may become stationary or turbulent, and

an entrained turbulent chimera state may become stationary (regularization).

Finally, one can consider a chimera on the *microscopic* level, where one looks at individual oscillators in a large, but finite set of Eq. (1). The transition to this level is highly nontrivial due to two reasons. First, even if one remains in the continuous limit of Eq. (2), the basic “stationary chimera” solution is no more periodic but quasiperiodic with infinitely many frequencies: individual oscillators in the coherent domain all have the basic frequency Ω_0 , but the frequencies in the incoherent domain are all different and fill an interval. We are not aware of any mathematical theory of synchronization for such objects. Practically, we can characterize synchronization at the microscopic level by determining average frequencies for all individual oscillators. An interesting feature, reported below, is the appearance of multiple steps in the frequency profiles for regimes outside of the main Arnold tongue. Second, the picture of a “stationary chimera” should be revised if instead of the continuous limit one considers a finite set of N oscillators. It is known that in such a system of ordinary differential equations (1) a chimera is a chaotic state with a nonzero largest Lyapunov exponent [14,15]. Thus, even synchronization of a “stationary chimera” should formally be considered as the phase synchronization of chaotic oscillations [13]. But this is not the end of the difficulties. The weakly chaotic chimera possesses a new, very large timescale of overall coherence; this time diverges in the continuous limit but is finite for finite system sizes N . Because of chaos, the coherent region in a chimera performs a random walk, so that on a very large timescale each oscillator at some epochs belongs to the coherent domain, and at some epochs belongs to the incoherent domain. This random walk restores symmetry to spatial shifts: now the mean frequencies of all oscillators are equal, and this frequency is not the basic frequency of the “stationary chimera” Ω_0 . We, however, will not explore such long timecales, which appear to be beyond computational availability for ensemble sizes $N = 4096$ and $N = 8192$ used in simulations below.

III. STATIONARY LOCKED CHIMERA STATES AND THEIR STABILITY

In this section we present a numerical procedure for finding standing locked chimeras of system (4) and (6) and determining the stability of these patterns. These chimeras are periodic in space solutions of the corresponding set of ordinary differential equations, describing spatial profiles of patterns rotating exactly with the external frequency Ω . This approach allows us to determine (with desired accuracy) the borders of the existence domain (Arnold tongue) of chimeras locked by the forcing, for a fixed length L of the medium. Below we describe the main steps of our method; details are discussed in the Appendixes.

We look for the locked patterns uniformly rotating with the frequency Ω of forcing:

$$Z(x, t) = z(x)e^{i\Omega t}, \quad H(x, t) = h(x)e^{i\Omega t}. \quad (7)$$

Substituting this in (4) and (6) yields a system of equations for the spatial profiles

$$e^{i\alpha} h^* z^2 + 2i\Omega z - e^{-i\alpha} h = 0, \quad h'' - h = -z - \varepsilon e^{i\alpha}. \quad (8)$$

Hereafter primes denote derivatives with respect to the spatial coordinate x . The first algebraic equation allows one to express z through h (where one of two roots is chosen according to the local stability condition [3,8,12,16,17]). Thus, we obtain the following ordinary differential equation for the complex function $h(x)$:

$$h'' - h = (\Omega + \sqrt{\Omega^2 - |h|^2})e^{i\beta}/h^* - i\varepsilon e^{-i\beta}, \quad (9)$$

where, for convenience of further notation, we define parameter $\beta = \pi/2 - \alpha$, measuring the deviation of α from $\pi/2$. We also stress that at the boundaries of the interval $[0, L]$, periodicity conditions $h(0) = h(L)$ and $h'(0) = h'(L)$ should be satisfied.

In order to find chimera states described by (9), we represent the complex field $h(x)$ in the form

$$h(x) = r(x)e^{i\theta(x)}, \quad (10)$$

where $r(x)$ and $\theta(x)$ are real variables depending on x . However, unlike the classic exponential form representation of a complex function, we accept that $r(x)$ can take both positive and negative values, and then $\theta(x)$ does not undergo jumps by $\pm\pi$ at the points where $r(x)$ becomes zero, but remains a smooth function passing through these points.

Substituting (10) into (9), equating to zero real and imaginary parts of the resulting expression, and introducing a new variable $q(x) = r^2(x)\theta'(x)$ for convenience, we get the following system of real ordinary differential equations of the fourth order, with parameters β , Ω , and ε :

$$\begin{aligned} r'' &= r + \frac{q^2}{r^3} + \frac{\Omega}{r} \cos \beta - \frac{\sqrt{r^2 - \Omega^2}}{r} \sin \beta - \varepsilon \sin(\theta + \beta), \\ q' &= \Omega \sin \beta + \sqrt{r^2 - \Omega^2} \cos \beta - \varepsilon r \cos(\theta + \beta), \\ \theta' &= q/r^2 \end{aligned} \quad (11)$$

in the domain where $|r(x)| \geq |\Omega|$, i.e., in the region of synchronous behavior of neighboring medium elements, and

$$\begin{aligned} r'' &= r + \frac{q^2}{r^3} + \frac{\Omega + \sqrt{r^2 - \Omega^2}}{r} \cos \beta - \varepsilon \sin(\theta + \beta), \\ q' &= (\Omega + \sqrt{r^2 - \Omega^2}) \sin \beta - \varepsilon r \cos(\theta + \beta), \\ \theta' &= q/r^2 \end{aligned} \quad (12)$$

in the domain where $|r(x)| < |\Omega|$, i.e., in the region of asynchronous or partially synchronous rotation of phase oscillators. When constructing solutions, we switch between (11) and (12) at $|r(x)| = |\Omega|$. Note the uniqueness of solutions is not violated because there are no solutions tangent to the set $|r(x)| = |\Omega|$.

Equations (9), (11), and (12) for the autonomous case ($\varepsilon = 0$) have been explored in Refs. [8,17] to find free (unforced) chimera patterns. The main difference with the free case is that the forcing term ε breaks the phase shift invariance $\theta \rightarrow \theta + \theta_0$, where θ_0 is an arbitrary constant. The latter invariance allowed us in the autonomous case to reduce the full fourth-order system (11) and (12) to a third-order system.

Our strategy (described in more detail in Appendixes A and B) is to find, for each pair of values ε , Ω , a symmetric

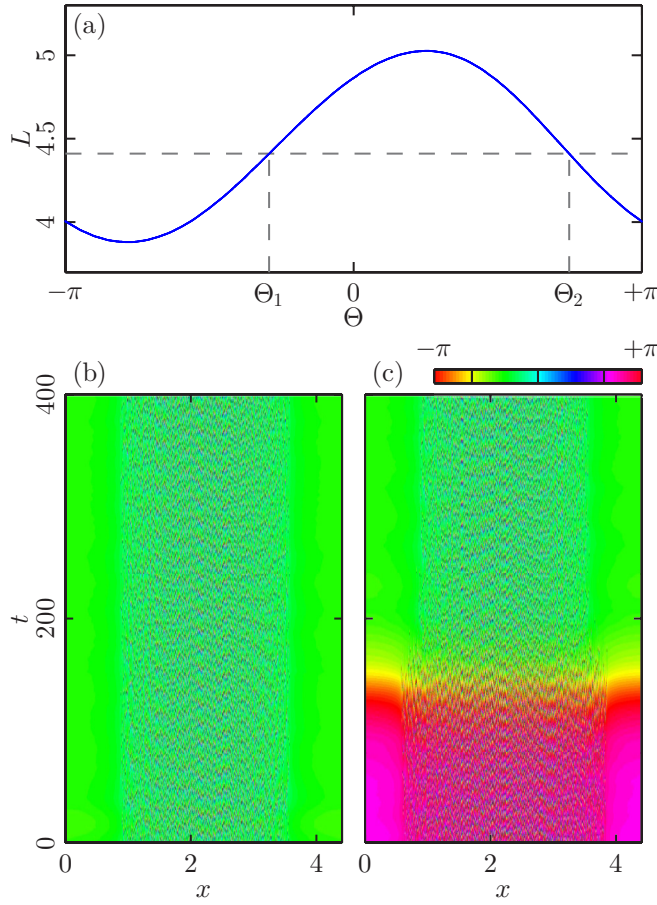


FIG. 1. (a) Dependence of the length $L(\Theta)$ of a chimera pattern on the phase shift parameter $\theta(0) = \Theta$ for $\Omega = -0.8$ and $\varepsilon = 0.025$. The horizontal dashed straight line corresponds to $L = \bar{L} = 4.41$. The vertical dashed lines depict values $\Theta_1 = -0.92$ and $\Theta_2 = 2.35$. (b, c) Direct numerical simulations of the set of $N = 4096$ oscillators, performed within the phase model (1). Spatiotemporal plots show the phases in the reference frame rotating with an angular velocity Ω for (b) $\Theta = \Theta_1$ (stable phase shift) and (c) $\Theta = \Theta_2$ (unstable phase shift).

periodic solution of (11) and (12) starting from a state $r(0) = R$, $\theta(0) = \Theta$, $r'(0) = 0$, $\theta'(0) = 0$. The “initial” value $r(0) = R$ is adjusted to find a periodic solution, the period of which L will depend on the “initial” phase $\theta(0) = \Theta$. As the dependence $L(\Theta)$ is a 2π -periodic function of Θ , in a certain range of system lengths $L_{\min} < L < L_{\max}$ we have at least two solutions for each L (in fact, in all cases presented below this number are exactly two because we consider only the 1:1 locking). We illustrate this in Fig. 1. In this figure we also show the long-time evolution of spatial profiles for both of the two possible periodically forced chimera states for $L = 4.41$. It is clearly seen that one of them (which corresponds to the phase shift $\Theta = \Theta_1 = -0.92$) is stable (the synchronization pattern does not change in course of evolution [Fig. 1(b)], and another one (which corresponds to the phase shift $\Theta = \Theta_2 = 2.35$) exhibits an unstable behavior (it evolves into the first one due to the corresponding instability development [see Fig. 1(c)]). This observation is in full correspondence with generic prop-

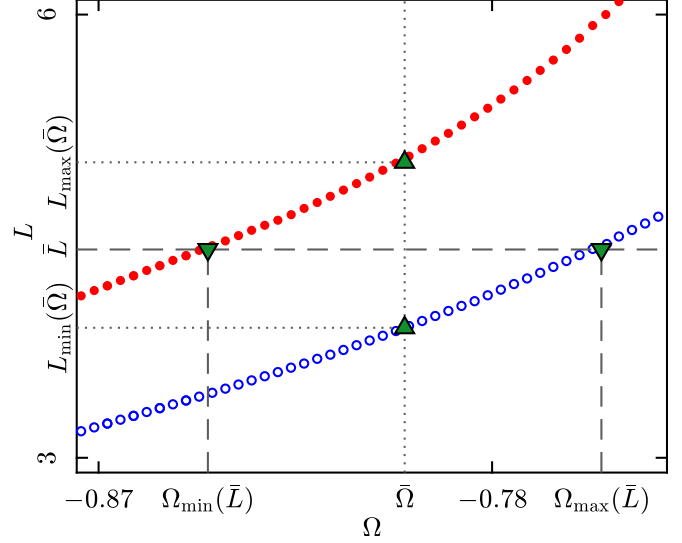


FIG. 2. Dependencies $L_{\max}(\Omega)$ (filled red circles) and $L_{\min}(\Omega)$ (open blue circles), numerically calculated for $\varepsilon = 0.025$. The upward-oriented triangular markers depict the values of L_{\min} and L_{\max} for $\Omega = \bar{\Omega} = -0.8$. The downward-oriented triangular markers show the values of Ω_{\min} and Ω_{\max} for a fixed length $L = \bar{L} = 4.41$ of the medium. The range between Ω_{\max} and Ω_{\min} determines the width of the Arnold tongue for $\varepsilon = 0.025$ in the case where $L = \bar{L} = 4.41$.

erties of the 1:1 locking, where there are two locked solutions, one phase-shift stable, and another phase-shift unstable.

The next step is determining from the data of Fig. 1(a) the values of $L_{\min}(\varepsilon, \Omega)$ and $L_{\max}(\varepsilon, \Omega)$ in a range of values of the forcing frequency Ω , for fixed ε . These curves are illustrated in Fig. 2. To find the borders of the Arnold tongue, i.e., the synchronization region, for a fixed length L of the medium, we have to inverse these dependencies as $\Omega_{\min}(\varepsilon, L)$ and $\Omega_{\max}(\varepsilon, L)$ (see Fig. 2 and Appendix B for details). Then the phased locked solutions for a chimera pattern in the system of length L exist in the Arnold tongue defined as $\Omega_{\min}(\varepsilon, L) < \Omega < \Omega_{\max}(\varepsilon, L)$. As $\varepsilon \rightarrow 0$, this tongue shrinks to the frequency $\Omega_0(L)$ of the autonomous chimera pattern. Examples of the Arnold tongues are presented in Fig. 3 (details of the dynamics inside of them will be discussed in Sec. IV).

Additionally, we have to check the general (not only the phase-shift) stability of the found patterns. To this end one linearizes the full system (4) and (6) and solves the eigenvalue problem. Practically, this can be done via a finite-difference representation described in Refs. [8,17–19] (see more detailed discussion in Appendix C), allowing for reducing the problem to that of finding eigenvalues of large matrices. The method yields reliable estimation of discrete eigenvalues, which are responsible for possible instabilities (see detailed discussion in Refs. [12,16]).

IV. EFFECT OF PERIODIC FORCING ON CHIMERAS OF DIFFERENT COMPLEXITY

A. Stable, breathing, and turbulent free chimeras

We first discuss different types of autonomous chimeras, and then describe how the external force governs them. The stability analysis as described in Appendix C also can be

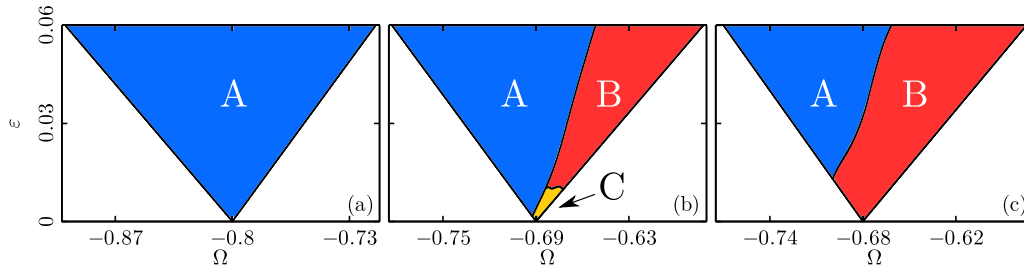


FIG. 3. Existence domains of the locked chimera patterns for (a) $L = 4.41$, (b) $L = 6.854$, and (c) $L = 7.332$. The corresponding natural frequencies of autonomous stationary chimeras are (a) $\Omega_0 = -0.8$ (stable), (b) $\Omega_0 = -0.69$ (unstable, evolves to a breather), and (c) $\Omega_0 = -0.68$ (unstable, evolves to a turbulent state); cf., Fig. 4. Inside of each presented Arnold tongue, in domain A (blue color) one of the two existing locked chimeras is stable. In regions B and C (red and yellow colors), all stationary chimeras are unstable, and the observed state is either turbulent in domain B or time-periodic (breathing chimera) in region C.

applied to autonomous chimera patterns [8,17–19], correspondingly one distinguishes stable and unstable unforced chimeras. The latter solutions evolve typically into breathing (time-periodic) [18–21] or turbulent chimeras [11,19]. These three possible regimes are illustrated in Fig. 4. Here we present the results of direct numerical simulation (panels a, b, and c) in the framework of the phase oscillator system (1) for parameters corresponding to cases of zero external force $\varepsilon = 0$, i.e., at the tip of the Arnold tongue. In Fig. 4 we also show the spatial profiles of functions $|z(x)|$ and $|h(x)|$ (panels d, e, and f), and the corresponding spectra of eigenvalues λ (panels g, h, and i). Point eigenvalues λ_p (red diamonds) are quite well separated from the seemingly continuous spectrum λ_c (violet circles), which does not have exactly a T -shaped form [12,16], but is distorted due to finite approximation effects (see Appendix C for details). For $\Omega_0 = -0.8$, the point spectrum λ_p satisfies condition $\text{Re}(\lambda_p) < 0$ [Fig. 4(g)], and a stable single-cluster chimera is realized in the phase model (1) [Fig. 4(a)]. For $\Omega_0 = -0.69$, a pair of complex conjugate numbers from a point spectrum exists with $\text{Re} \lambda_p > 0$ [Fig. 4(h)], a stationary chimera is therefore unstable, and a breathing chimera is observed in the system (1) [Fig. 4(b)]. For $\Omega_0 = -0.68$, a pair of complex conjugate point eigenvalues has even larger real parts [Fig. 4(i)]; here the unstable stationary chimera evolves to a turbulent regime with irregular dynamics of phases [Fig. 4(c)]. Below we show how an external forcing acts on these states.

B. Locking of a stable chimera

Here we consider the effect of external periodic forcing on a stable chimera. We exemplify this case with parameters $L_0 = 4.41$, $\Omega_0 = -0.8$ [Figs. 4(a), 4(d), and 4(g)]. For small forcing amplitudes $\varepsilon \lesssim 0.05$, we obtain a “standard” Arnold tongue on the plane ε, Ω , inside of which a locked chimera is stable [see Fig. 3(a)]. The dynamics of locking is illustrated in Fig. 5(b). Here we show the phases of the oscillators in a free-running state until time $t_0 = 500$, at which time the forcing with frequency $\Omega = -0.83$ and amplitude $\varepsilon = 0.025$ is applied. The phases are shown in the reference frame rotating with the external frequency Ω , and thus for $t < t_0$ one observes rotation of the phase in the synchronous domain. The effect of locking is evident by inspection of the phase difference between the external force and the coherent

domain for $t > t_0$: in the locked state it is constant. This corresponds to the shift of the profile of average frequencies of all the oscillators [Fig. 5(e)]: the whole profile shifts, so that the frequency of the coherent domain becomes exactly the external one (depicted by the dotted line). It is noteworthy that the size of the regular domain increases under forcing.

Outside of the locking region (i.e., for a large mismatch between Ω and Ω_0), one observes unlocked quasiperiodic regimes [Figs. 5(a) and 5(c)]. For $\Omega < \Omega_0$, all the oscillators have frequencies larger than Ω , and one can clearly see the plateaus at the modulation frequency and its harmonics in the profile of average frequencies [Fig. 5(d)]. For $\Omega > \Omega_0$, the major part of the coherent oscillators have a frequency less than Ω , but there exists another plateau exactly at the driving frequency [Fig. 5(f)]. Remarkably, the phases of these oscillators, in the reference frame rotating with Ω , are not constants, but experience rather large variations (see Fig. 6); nevertheless, they are perfectly frequency entrained by the force. The existence of the plateaus in the frequency profile resembles that for breathing chimeras [18,20,22]. In the latter case, however, an extra modulation frequency appears due to the instability of the stationary chimera; in our case the modulation frequency is due to the imperfect locking to the external field.

C. Stabilization of a breathing chimera

Next we consider how the periodic force affects a breathing chimera. The latter exists for parameters $L_0 = 6.854$, $\Omega_0 = -0.69$. Here the stationary chimera state is weakly unstable with two discrete complex eigenvalues having a positive real part. In the autonomous, unforced situation, a breathing, time-periodic state appears. Here also the Arnold tongue can be constructed as described above. However, only in part A of this locked region is the constructed stationary chimera state stable. In part B of the Arnold tongue colored red in Fig. 3(b), the constructed stationary chimera state is unstable and evolves into a turbulent chimera. We illustrate these two situations in Fig. 7. It shows two regimes, one of a stable locked chimera (panels a, c, and e), and one of an unstable chimera (panels b, d, and f), for two points inside the Arnold tongue Fig. 3(b).

For very small forcing, the locked chimera inherits the instability of the autonomous chimera and evolves into a

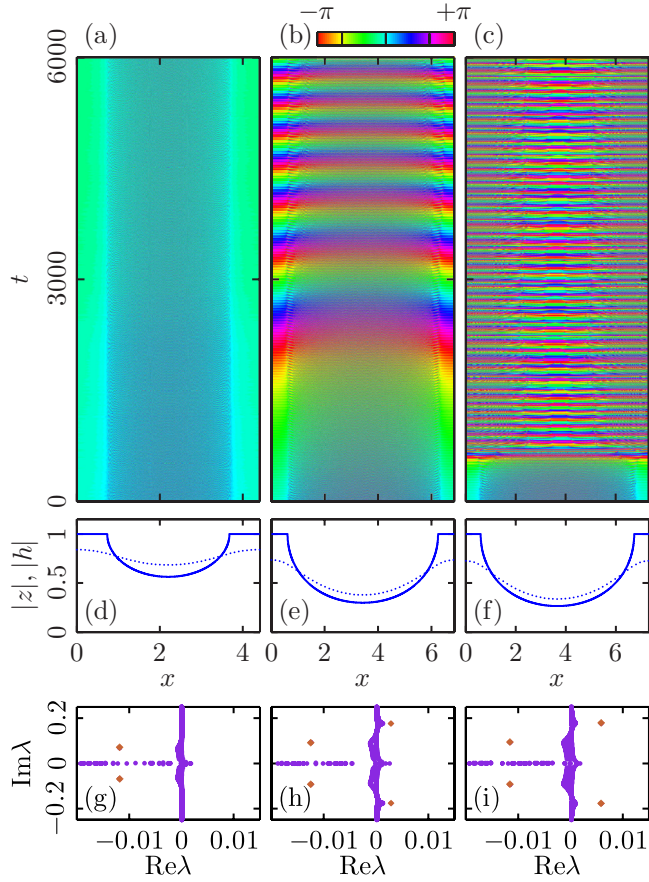


FIG. 4. Dynamics of the system (1) in the autonomous case $\varepsilon = 0$. Panels (a)–(c) show a space-time plot of the phases in the reference frame rotating with angular velocity Ω_0 . Panels (d)–(f) depict profiles $|z(x)|$ (solid line) and $|h(x)|$ (dotted line), found with the method of Sec. III, and determining the initial phase distribution for a numerical simulation. Panels (g)–(i) demonstrate the spectrum λ of linear perturbations of solutions (7) of Eqs. (4) and (5). Violet circles are the eigenvalues of the finite-size matrices, not corresponding to the discrete part of the spectrum. Because of a finite discretization, this set consists not only of purely real negative and purely imaginary numbers, although it has the characteristic T shape. Red diamonds are eigenvalues belonging to the point spectrum λ_p responsible for instability. (a, d, g) Stable chimeric for $\Omega_0 = -0.8$, $L = 4.41$. (b, e, h) Breathing chimeric state for $\Omega_0 = -0.69$, $L = 6.854$. (c, f, i) Turbulent regime for $\Omega_0 = -0.68$, $L = 7.332$.

breathing state [a tiny yellow region C close to the tongue tip in Fig. 3(b)]. In Fig. 8 we illustrate with the phases [Fig. 8(a)] and with the order parameter [Fig. 8(b)] how a breathing state develops into a stable stationary chimeric for a not-so-small forcing. One can clearly observe the free breathing chimeric up to time $t_0 = 1000$, at which the forcing is switched on. Then, for $t > t_0$, the mean frequency becomes locked by the force, and periodic modulations of the order parameter disappear, which means establishing of a standard stationary chimeric state.

Figure 9 provides a more detailed characterization of regimes at larger values of forcing. Locking properties of the chimeric pattern are characterized by the phase of the global complex order parameter $\bar{Z} = N^{-1} \sum_{n=1}^N e^{i\varphi_n} = \bar{R} e^{i\bar{\varphi}}$.

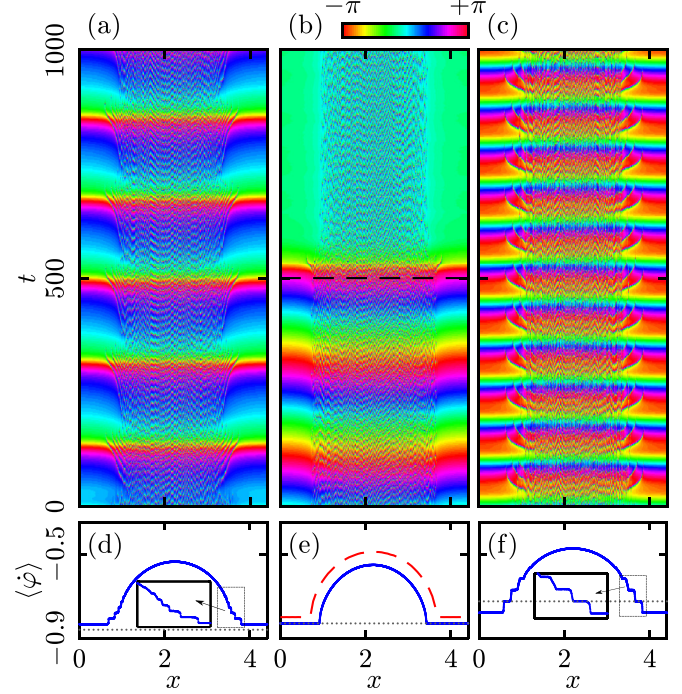


FIG. 5. Locking of a stable chimeric. Direct numerical simulations of the set of $N = 4096$ oscillators performed within the phase model (1) with parameters $\varepsilon = 0.025$ and different driving frequencies: (a, d) $\Omega = -0.86$, (b, e) $\Omega = -0.83$, and (c, f) $\Omega = -0.725$. Panels (a)–(c) show spatiotemporal plots of the phases in the reference frame rotating with the driving frequency Ω . Panels (d)–(f) demonstrate average frequencies of the elements (blue lines) together with the forcing frequency Ω (gray dotted line); insets in panels (d) and (f) enlarge plateaus on frequency profiles. In each case, the initial state was close to the autonomous chimeric state at the length $L = 4.41$ and the corresponding natural frequency $\Omega_0 = -0.8$. For situations depicted in panels (a) and (c), the external force was presented during the full simulation time. In the case shown in panel (b), the force was switched on abruptly at the time instant $t_0 = 500$ (black dashed straight line in panel (b)). A red dashed curve in panel (e) shows a profile of average frequencies of the oscillators for a free-running chimeric state.

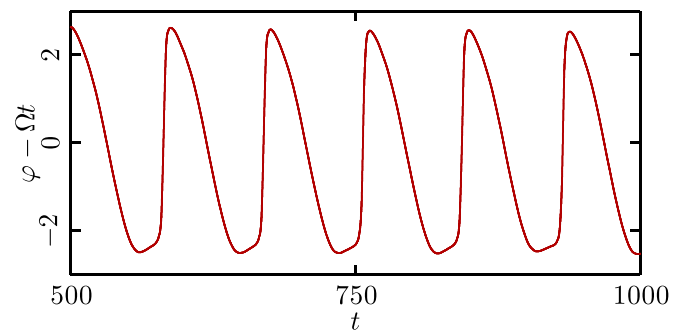


FIG. 6. Phase (in the reference frame rotating with the force frequency Ω) vs time for the oscillator belonging to the subgroup entrained by the external force. The diagram shows the dynamical behavior of the element located at $x = 0.64$ in the numerical simulation corresponding to Figs. 5(c) and 5(f).

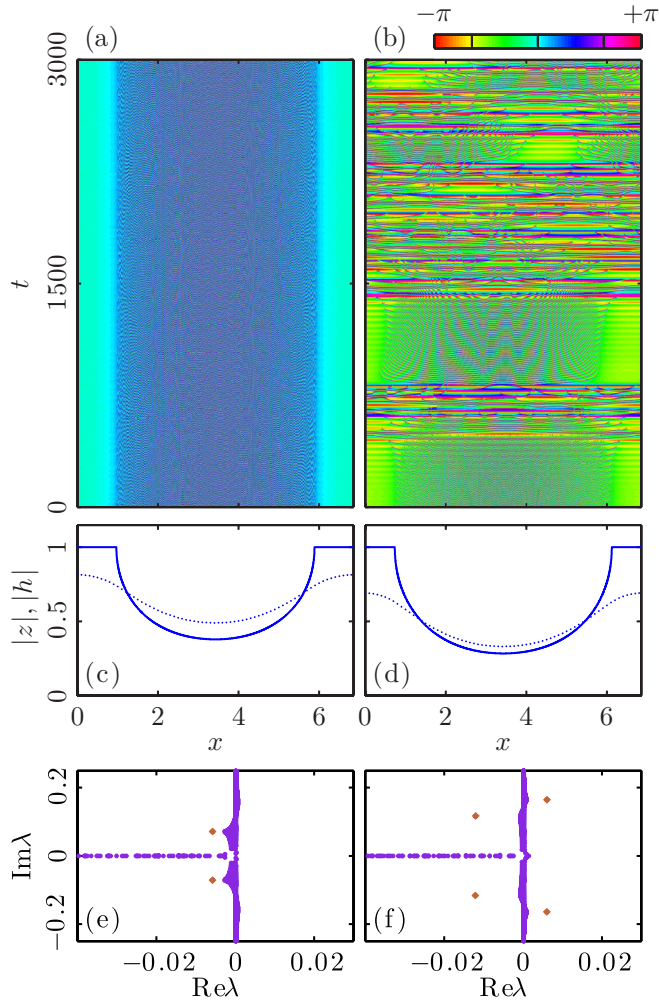


FIG. 7. Synchronization of a breathing chimera. Panels (a) and (b) show a space-time plot of the phases in the reference frame rotating with the driving frequency Ω for $L = 6.854$. Panels (c) and (d) depict profiles $|z(x)|$ (solid line) and $|h(x)|$ (dotted line), found with the method of Sec. III, and determining the initial phase distributions for numerical simulations. Panels (e) and (f) demonstrate the spectrum λ of linear perturbations for the corresponding solutions. Violet circles are the eigenvalues of discrete matrices not corresponding to the discrete part of the spectrum. Red diamonds are eigenvalues belonging to the point spectrum λ_p responsible for instability. (a, c, e) Stable chimera for $\Omega = -0.74$, $\varepsilon = 0.05$. (b, d, f) Turbulent regime for $\Omega = -0.63$, $\varepsilon = 0.05$.

We calculated the global observed frequency $\Omega_{\text{obs}} = \langle \dot{\theta} \rangle$ and compared it to the driving frequency Ω . In parallel, we calculated the standard deviation of the global real order parameter \bar{R} from a mean value. The latter observable provides a reliable characterization of regularity of the chimera; for regular patterns it is very small, while it has finite values for turbulent and time-periodic patterns. Inspection of Fig. 9 reveals that domains of frequency locking (where $\Omega_{\text{obs}} = \Omega$) and regularity coincide. This means that in a disordered state inside the domain B of Fig. 3(b), the chimera on average is not locked, although temporary locked patches may be observed (see Fig 7). The standard deviation of the global real order parameter is a good indicator of the existence of stationary

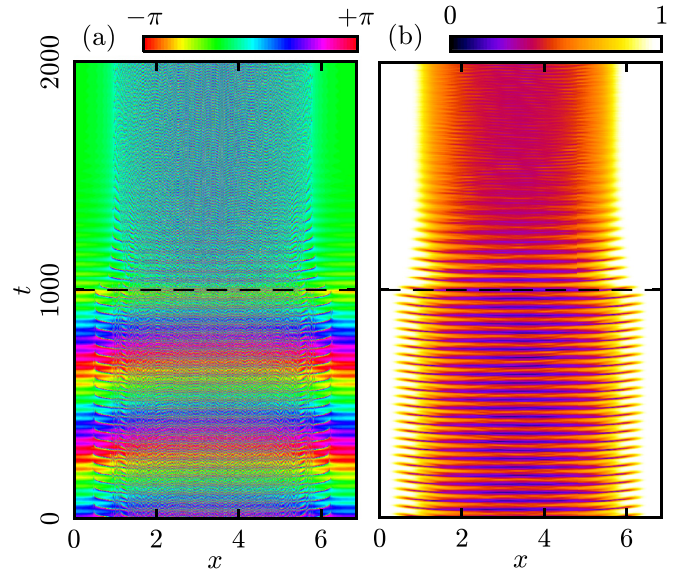


FIG. 8. Synchronization of breathing chimera for $L = 6.854$. (a) Spatial distribution of the phases in the reference frame rotating with the driving frequency Ω . (b) Absolute value $|Z(x, t)|$ of the complex order parameter. Numerical simulations of the set of $N = 8192$ oscillators were performed within the framework of the phase model (1) with $\varepsilon = 0.06$, $\Omega = -0.69$. The initial conditions were chosen in the form of an unforced breathing chimera state. The force was switched on abruptly at the time instant $t_0 = 1000$, as marked by a black dashed straight line. The coarse-grained order parameter $Z(x, t)$ was calculated via local averaging with a Gaussian kernel $\exp(-x^2/2\zeta^2)$, with $\zeta = 0.1$.

chimera (where this quantity is very small), and thus it was used to draw boundaries of region A in Fig. 3. However, this quantity cannot differentiate turbulent and periodic states (which is needed to draw a border between regions B and C). Here just a visual inspection of the time series $\bar{R}(t)$ [see Fig. 9(c)] was adopted. Because of finite-size effects, periodicity in the breathing state C is not perfect, and thus the border between regions B and C should be considered as a fuzzy one.

Figure 9 shows that the locking of chimeras occurs in blue domains A of Fig. 3 only. Loss of locking can happen in two ways. At small values of Ω the locking-unlocking transition happens exactly at the values where the locked solution disappears (left boundary of the triangle region in Fig. 3). At large values of Ω , the transition to turbulent state (red domain B) is simultaneously the locking-unlocking transition. In Fig. 3 we did not color the states outside of the triangular existence domain of stationary locked solutions; however, Fig. 9 shows that there is not any regime change at the right border of red domain B ; the turbulent unlocked state just continues to exist at larger values of Ω .

D. Regularization of a turbulent chimera state

Finally, we discuss regularization of a turbulent chimera. The latter is observed for $L_0 = 7.332$, $\Omega_0 = -0.68$. Here the instability of a free chimera solution is so strong that a disordered state, where the local order parameter fluctuates in space and time, is observed. The calculated Arnold tongue is presented in Fig. 3(c). Again, the domain of existence of

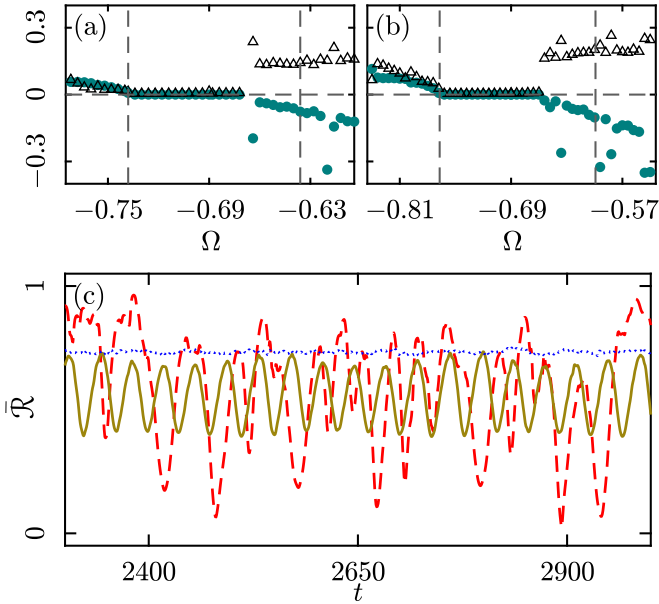


FIG. 9. (a, b) Dependencies of the frequency difference $\Omega_{\text{obs}} - \Omega$ (filled circles) and the standard deviation of the global real mean field $\bar{\mathcal{R}}$ fluctuations (triangles) for the case of a forced breathing chimera of Fig. 3(b), in a lattice of $N = 4096$ units. (a) $\varepsilon = 0.03$, (b) $\varepsilon = 0.05$. Dashed horizontal line shows zero level; dashed vertical lines are borders of existence of the locked solution [bold black lines in Fig. 3(b)]. One can see that transition to turbulence (at the right side of the panels) is rather abrupt and immediately leads to a deviation of the observed frequency from the forced one. (c) Time series of the global real mean field $\bar{\mathcal{R}}(t)$ for a stationary chimera (dotted blue line), for a periodic chimera (solid brown line) and for a turbulent chimera (dashed red line).

a locked stationary chimera looks like a standard triangular synchronization domain, but only in a relatively small part A (blue region) is this solution stable. We illustrate this situation with the evolution of the order parameter in Fig. 10(b). A turbulent chimera is observed prior to the force onset time $t_0 = 1500$, where under forcing it is transformed to a stable stationary chimera.

For larger values of the driving frequency [red region B in Fig. 3(c)], locked solutions in the presence of driving typically inherit the instability of the free chimera, so that also under periodic forcing are turbulent states observed [Fig. 10(a)]. Dependencies of the global frequency and of the standard deviation of the global order parameter are similar to those presented in Fig. 9. We stress here, that for very large forcing amplitudes, an observed turbulent state is a transient one, evolving after a long irregular evolution into an absorbing fully synchronized regime.

V. CONCLUSION

Summarizing, we studied the effect of a periodic forcing on a chimera state in a one-dimensional medium. We have constructed stationary locked chimera patterns as periodic in space and time profiles via solutions of a proper ordinary differential equation. The simplest picture is observed if the free chimera is stable. Here the macroscopic effect of forcing

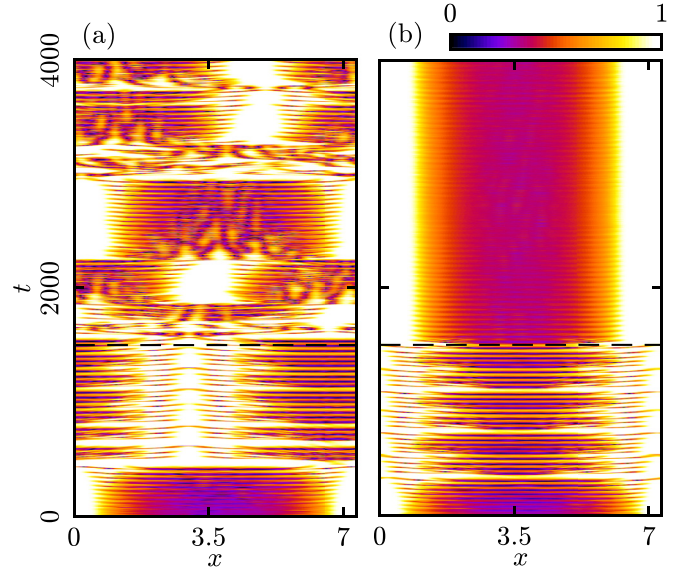


FIG. 10. Synchronization of turbulent chimera for $L = 7.332$. The dynamics of amplitude of the local complex order parameter $|Z(x, t)|$ calculated as in Fig. 8 in direct numerical simulations of the set of $N = 8192$ oscillators within the phase model (1) with the parameters (a) $\varepsilon = 0.03$, $\Omega = -0.68$, and (b) $\varepsilon = 0.06$, $\Omega = -0.68$. The initial conditions were chosen in the form of a stationary chimera solution, which develops due to the instability into a turbulent state. The force was switched on abruptly at the time instant $t_0 = 1500$, which is marked by a black dashed straight line. One can see that a large enough forcing can stabilize and regularize the behavior of the system, which evolves to a standard chimera regime (see panel b).

on it is very similar to a general synchronization setup: there is a locking region within which the chimera is locked by the forcing, while outside of the Arnold tongue a quasiperiodic dynamics is observed. Inside the Arnold tongue, on the mesoscopic level, one observes enlargement of the synchronized domain. On the microscopic level of individual oscillators, no essential changes are observed inside the Arnold tongue. However, the dynamics on the microscopic level becomes nontrivial outside the Arnold tongue, with several plateaus of oscillators subgroups appearing. In particular, we observed that while the basic frequency of the chimera is not entrained, some groups of oscillators may be entrained to the external frequency, and for these units quite large variations of the phase difference from the forcing one are observed despite frequency entrainment.

At the mesoscopic level of the spatiotemporal dynamics of the coarse-grained order parameter, we described the effect of regularization of nonstationary chimeras, breathing or turbulent; such an effect does not exist in simple synchronization setups. Here, inside the Arnold tongue there are subdomains, at sufficiently strong coupling, where external forcing stabilizes a stationary chimera. On the contrary, in some domains a weakly nonstationary (breathing) chimera may become turbulent due to forcing, but still with an entrained basic frequency.

Our approach is based on the explicit construction of the phase-locked solutions and on the analysis of their stability. Then these conclusions are checked in direct numerical simulations of the basic set of phase equations. In this way our

study differs from the approach of Refs. [6,7] where comprehensive direct numerical simulations of two coupled chimera ensembles have been performed, and regimes of phase locking between them (or their mean fields) identified. Direct simulations of forced chimera states seems to be the only possibility in cases, where it is hard to find chimera profiles and to analyze their stability, like in an example studied in Refs. [23,24].

An extension of the presented approach to the cases where the interaction kernel is not exponential, but a sum of a few Fourier harmonics (like in Ref. [22]) would potentially simplify the stability analysis; however, in the present paper we focused on the “classical” Kuramoto-Battogtokh case [1]. Furthermore, potentially high-order Arnold tongues may also exist (in another system they have been observed in Refs. [23,24]), but construction of such solutions appears hardly possible with our methods, because they are not stationary in the reference frame rotating with the external frequency.

ACKNOWLEDGMENTS

This paper was supported by the Russian Science Foundation (study of turbulent chimeras, Sec. **IV D**, Grant No. 17-12-01534) and the Russian Foundation for Basic Research (study of stationary and breathing chimeras, Secs. **IV B** and **IV C**, Grant No. 19-52-12053). A.P. was partially supported in development of numerical methods (Appendixes **A** and **B**) by the Laboratory of Topological Methods in Dynamics NRU HSE, of the Ministry of Science and Higher Education of the Russian Federation, Grant No. 075-15-2019-193. The authors thank O. Omelchenko and R. G. Andrzejak for helpful discussions.

APPENDIX A: DETAILS OF NUMERICAL METHOD OF FINDING STATIONARY CHIMERA PATTERNS

Here we describe our numerical chimera-seeking approach based on Eqs. (11) and (12). The goal is to find period- L solutions $r(x)$, $r'(x)$, $q(x)$, and $\theta(x)$. [Note that in this work we confine ourselves to the analysis of stationary profiles of macroscopic fields without any twist of the phase when passing across the entire medium, i.e., we discuss only cases where $\theta(L) = \theta(0)$, while in general solutions with $\theta(L) = \theta(0) + 2\pi m$, where m is integer, are also admissible.] Furthermore, because of the invariance with respect to spatial shifts and the observation that the force-free chimera patterns are symmetric, we seek solutions in the class of symmetric functions $r(x)$, $\theta(x)$ and antisymmetric functions $r'(x)$, $q(x)$, where symmetry is defined with respect to the point $x = L/2$. For such solutions of system (11) and (12), by virtue of the periodic boundary conditions, the equalities $r(0) = r(L)$ and $q(0) = q(L)$ should be fulfilled only if $r'(x)$ and $q(x)$ vanish at points $x = 0$, $x = L/2$, and $x = L$. In our previous work [8,17–19] we demonstrated that in the case where an external force is absent, i.e., $\varepsilon = 0$, for a given parameter Ω these constraints determine the value of L and the possible form of the functions $r(x)$, $r'(x)$, and $q(x)$ [and therefore also $\theta(x)$ and the complex field $h(x)$] that is exactly repeated with the period L . As has been discussed in Refs. [8,17–19] for the autonomous

case $\varepsilon = 0$, it is convenient to fix the basic frequency of the pattern Ω , and find periodic solutions, the period of which $L(\Omega)$ is the function of this parameter.

In the case $\varepsilon = 0$ the dimension of the system of real ordinary differential equations (11) and (12) can be reduced because Eq. (9) is invariant to a constant phase shift of the complex field $h(x)$. Hence, the function $\theta(x)$ is defined up to an arbitrary constant shift θ_0 . An external uniform force with amplitude $\varepsilon \neq 0$ and frequency Ω in the right-hand side of (2) breaks the phase shift invariance of Eq. (9). If $\varepsilon \neq 0$, it is required to consider the full system of four-order ordinary differential equations (11) and (12) and to find its periodic solutions. Now our strategy consists of two main steps, which are as follows.

First, we look for symmetric periodic trajectories in the phase space of the system (11) and (12) for fixed values of parameters ε , Ω and for a fixed value Θ of the phase at $x = 0$. We employ the shooting method [25]: Eqs. (11) and (12) are solved numerically (using the Runge-Kutta method of fourth order [25]) with “initial” conditions $r(0) = R$, $r'(0) = 0$, $q(0) = 0$, and $\theta(0) = \Theta$ at the starting point $x = 0$. Integration ends at a point $x = \ell$, where the condition $r'(\ell) = 0$ is fulfilled. To satisfy the condition $q(\ell) = 0$, one has to vary the remaining free parameter R . Its value can be found using a root-finding method [25]. This found value R determines profiles $r(x)$, $r'(x)$, $q(x)$, and $\theta(x)$, which are periodic with length $L = 2\ell$. This length $L = 2\ell$ depends on the parameters ε , Ω (and also α) of Eqs. (11) and (12) and on a value of the “initial” phase Θ . In this way, one can obtain the chimera length as a function $L(\varepsilon, \Omega, \Theta)$ of three variables. An example of this calculation is seen in Fig. 1(a).

At the next stage of the numerical procedure, we set $L = 2\ell$, substitute the previously chosen values of ε , Ω into Eq. (9) and solve it numerically on the interval $[0, L)$, taking $h(0) = Re^{i\Theta}$ and $h'(0) = 0$ as “initial” conditions. As a result, we find the profile $h(x)$, which corresponds to the standing chimera state for the locally coupled phase oscillators distributed continuously over an interval of length $L = 2\ell$ with periodic boundary conditions.

Noteworthy, the function $h(x)$ has to satisfy the conditions of periodicity $h(L) = h(0) = Re^{i\Theta}$ and $h'(L) = h'(0) = 0$. Thus, this fact allows us to additionally check that the solution $h(x)$ we obtain numerically can be associated with a pattern existing in oscillatory medium closed to the ring. Finally, we note that the proposed method can be employed in the case of chimeras with any number of synchronous regions, choosing the corresponding point where $r'(x)$ and $q(x)$ vanish simultaneously.

APPENDIX B: ARNOLD TONGUE FOR LOCKED CHIMERAS

Here we describe how the found chimera patterns are attributed to certain domains of Ω , ε at a given medium length L . According to Appendix A, $L(\varepsilon, \Omega, \Theta)$ is a 2π -periodic function of Θ if $\varepsilon \neq 0$. Hence, in a certain range of system length $L_{\min}(\varepsilon, \Omega) < L < L_{\max}(\varepsilon, \Omega)$ we have at least two solutions for each L [cf., Fig. 1(a)]. On the other hand, in the absence of forcing, i.e., when $\varepsilon = 0$, Eqs. (11) and (12) have the property of phase shift invariance $\theta \rightarrow \theta + \theta_0$, so the

function $L(0, \Omega, \Theta)$ does not depend on the “initial” phase Θ at the point $x = 0$. In this situation, for the fixed value of $\Omega = \Omega_0$ we can set $\Theta = 0$ and consider only a solution with $L = L(0, \Omega_0, 0)$. This defines a relation between the frequency Ω_0 of uniformly rotating autonomous chimera and the length L of the medium.

Next, we fix the value \bar{L} as one that possesses a stable or unstable unforced chimera state with the basic frequency Ω_0 . Hence, from the found patterns we have to select those having period \bar{L} . For fixed parameters ε , Ω , this reduces to an additional one-dimensional root-finding problem which is easy to accomplish [25]. For example, in Fig. 1(a) the value $\bar{L} = 4.41$, corresponding to the frequency $\Omega_0 = \bar{\Omega} = -0.8$, is depicted by the horizontal dashed straight line. It is clearly seen that two phases $\Theta_1 = -0.92$ and $\Theta_2 = 2.35$ exist, for which $L(\varepsilon, \Omega, \Theta) = \bar{L}$. Existence of at least two solutions is a must, as at locking of periodic oscillations by an external force there are typically two locking states, one stable and one unstable. Such stably and unstably locked synchronization patterns are demonstrated in Figs. 1(b) and 1(c), respectively.

To obtain the boundaries of chimera locked domains for fixed L , we determine functions $L_{\min}(\varepsilon, \Omega)$ and $L_{\max}(\varepsilon, \Omega)$ as the minimum and maximum of curves $L(\varepsilon, \Omega, \Theta)$ for given Ω , ε . Next, for a given length L , we have to inverse these dependencies as $\Omega_{\min}(L, \varepsilon)$ and $\Omega_{\max}(L, \varepsilon)$, which would then correspond to the left and right boundaries of the locked domain, respectively (see Fig. 2). In other words, if for fixed values ε , Ω and some L the inequalities $\Omega_{\min}(L, \varepsilon) < \Omega(L) < \Omega_{\max}(L, \varepsilon)$ are satisfied, then the point ε , Ω lies in the locked domain of the unforced (free) chimera existing in the medium of length L . The natural frequency of this chimera Ω_0 is determined from the condition $L = L(0, \Omega_0, 0)$. We present three locked domains (Arnold tongues) for static chimera states in media with three different lengths in Fig. 3.

APPENDIX C: STABILITY ANALYSIS OF CHIMERA STATE

Here we outline the linear stability analysis of the stationary chimera patterns. Temporal stability of the standing chimera state (7) uniformly rotating with the frequency Ω can be studied by linearizing the integral-differential equation (4) and (5) near the solution (7). For this purpose we assume that the local complex order parameter $Z(x, t)$ has the following form:

$$Z(x, t) = [z(x) + \mathcal{Z}(x, t)]e^{i\Omega t}, \quad (\text{C1})$$

where $\mathcal{Z}(x, t)$ describes x -periodic small deviations from the chimera profile $z(x)$. After the substitution of the expression (C1) into Eq. (4) and the linearization of the result with respect to the variations $\mathcal{Z}(x, t)$, we arrive at

$$\partial_t \mathcal{Z} = -[i\Omega + e^{i\alpha} z(x) h^*(x)] \mathcal{Z} + [e^{-i\alpha} \mathcal{H} - e^{i\alpha} z^2(x) \mathcal{H}^*] / 2, \quad (\text{C2})$$

where $\mathcal{H}(x, t)$ is the coupling force for $\mathcal{Z}(x, t)$ defined in terms of the convolution operator

$$\mathcal{H}(x, t) = \int_0^L G(x - \bar{x}) \mathcal{Z}(\bar{x}, t) d\bar{x}. \quad (\text{C3})$$

Next, we rewrite Eq. (C2) together with (C3) in the form of a linear operator equation

$$\partial_t \boldsymbol{\zeta} = (\hat{\mathbf{M}} + \hat{\mathbf{K}}) \boldsymbol{\zeta} \quad (\text{C4})$$

for the two-component vector function $\boldsymbol{\zeta}(x, t)$ consisting of the real $\zeta_1(x, t)$ and imaginary $\zeta_2(x, t)$ parts of the complex function $\mathcal{Z}(x, t) = \zeta_1(x, t) + i\zeta_2(x, t)$. Here $\hat{\mathbf{M}}$ is a multiplication operator

$$\hat{\mathbf{M}} \boldsymbol{\zeta} = \begin{pmatrix} \mu_1(x) & -\mu_2(x) \\ \mu_2(x) & \mu_1(x) \end{pmatrix} \begin{pmatrix} \zeta_1(x, t) \\ \zeta_2(x, t) \end{pmatrix} \quad (\text{C5})$$

and $\hat{\mathbf{K}}$ is an integral operator

$$\hat{\mathbf{K}} \boldsymbol{\zeta} = \begin{pmatrix} \varkappa_{11}(x) & \varkappa_{12}(x) \\ \varkappa_{21}(x) & \varkappa_{22}(x) \end{pmatrix} \int_0^L G(x - \bar{x}) \begin{pmatrix} \zeta_1(\bar{x}, t) \\ \zeta_2(\bar{x}, t) \end{pmatrix} d\bar{x}. \quad (\text{C6})$$

For convenience and brevity of the provided above representations of $\hat{\mathbf{M}}$ and $\hat{\mathbf{K}}$, we have introduced the above two real functions into (C5):

$$\begin{aligned} \mu_1(x) &= -\text{Re}[e^{i\alpha} z(x) h^*(x)], \\ \mu_2(x) &= -\text{Im}[e^{i\alpha} z(x) h^*(x)] - \Omega, \end{aligned} \quad (\text{C7})$$

and the following notations into (C6):

$$\begin{aligned} \varkappa_{11}(x) &= \{\cos \alpha - \text{Re}[e^{i\alpha} z^2(x)]\} / 2, \\ \varkappa_{12}(x) &= \{\sin \alpha - \text{Im}[e^{i\alpha} z^2(x)]\} / 2, \\ \varkappa_{21}(x) &= \varkappa_{12}(x) - \sin \alpha, \quad \varkappa_{22}(x) = \cos \alpha - \varkappa_{11}(x). \end{aligned} \quad (\text{C8})$$

It is noteworthy that for the continuous profiles $z(x)$ and $h(x)$ under consideration and any piecewise-smooth kernel $G(x)$, definitions (C5) and (C6) imply that both operators $\hat{\mathbf{M}}$ and $\hat{\mathbf{K}}$ are bounded, and, in addition, the integral operator $\hat{\mathbf{K}}$ is compact [12].

According to Eq. (C4), stability of the chimera state is determined by the spectrum of the eigenvalues λ of the linear time-independent composite operator $\hat{\mathbf{M}} + \hat{\mathbf{K}}$. As follows from the general spectral theory of linear operators, this spectrum λ is symmetric with respect to the real axis of the complex plane and consists of two different parts, a continuous spectrum λ_c and a point spectrum λ_p (see Refs. [12,16] for details). According to these references, the temporal stability of the standing chimera states is determined only by the point spectrum λ_p of the composite operator $\hat{\mathbf{M}} + \hat{\mathbf{K}}$. To identify the point spectrum, we use the approach suggested earlier by us in Refs. [8,17] and successfully employed in Refs. [18,19,21]. The main idea of this approach is based on the observation that the procedures of spatial discretization and replacement of integrals by large-dimension matrices (in particular, the choice of discretization points) hardly affect the point eigenvalues λ_p . This property of λ_p allows one to determine the point spectrum λ_p reliably for most values of the parameters L , α , ε , and Ω of the model (1) by repeatedly solving the approximate matrix eigenvalue problem (see Refs. [8,17,26]).

It should be mentioned that another approach for the study of the perturbation spectrum for chimera states, based on the Galerkin approximation of the solution with some basis functions, has been outlined in Ref. [12]. However, to the best of our knowledge, this method has been successfully applied to the chimeras with a harmonic interaction kernel only, where the problem can be reduced to a finite-dimensional one. It

would be interesting to implement the Galerkin method [12] to the problem considered in this paper and to compare results. In this respect we mention calculations of the perturbation spectrum in a two-dimensional setup in Ref. [27], where,

however, a dissipative (i.e., corresponding to an ensemble of nonidentical oscillators) version of the Ott-Antonsen equations was treated, so that the essential spectrum was separated from the imaginary axis.

-
- [1] Y. Kuramoto and D. Battogtokh, *Nonlinear Phenom. Complex Syst.* **5**, 380 (2002).
- [2] M. J. Panaggio and D. M. Abrams, *Nonlinearity* **28**, R67 (2015).
- [3] O. E. Omel'chenko, *Nonlinearity* **31**, R121 (2018).
- [4] C. Bick and E. A. Martens, *New J. Phys.* **17**, 033030 (2015).
- [5] G. Ruzzene, I. Omelchenko, E. Schöll, A. Zakharova, and R. G. Andrzejak, *Chaos* **29**, 051103 (2019).
- [6] R. G. Andrzejak, G. Ruzzene, and I. Malvestio, *Chaos* **27**, 053114 (2017).
- [7] R. G. Andrzejak, G. Ruzzene, I. Malvestio, K. Schindler, E. Schöll, and A. Zakharova, *Chaos* **28**, 091101 (2018).
- [8] L. Smirnov, G. Osipov, and A. Pikovsky, *J. Phys. A* **50**, 08LT01 (2017).
- [9] E. Ott and T. M. Antonsen, *Chaos* **18**, 037113 (2008).
- [10] C. R. Laing, *Physica D* **238**, 1569 (2009).
- [11] G. Bordugov, A. Pikovsky, and M. Rosenblum, *Phys. Rev. E* **82**, 035205(R) (2010).
- [12] O. E. Omel'chenko, *Nonlinearity* **26**, 2469 (2013).
- [13] A. S. Pikovsky, M. G. Rosenblum, G. V. Osipov, and J. Kurths, *Physica D* **104**, 219 (1997).
- [14] O. E. Omel'chenko, M. Wolfrum, and Y. L. Maistrenko, *Phys. Rev. E* **81**, 065201(R) (2010).
- [15] M. Wolfrum and O. E. Omel'chenko, *Phys. Rev. E* **84**, 015201(R) (2011).
- [16] J. Xie, E. Knobloch, and H.-C. Kao, *Phys. Rev. E* **90**, 022919 (2014).
- [17] L. A. Smirnov, G. V. Osipov, and A. Pikovsky, *Chimera patterns in one-dimensional oscillatory medium*, in *Nonlinear Waves and Pattern Dynamics*, edited by N. Abcha, E. Pelinovsky, and I. Mutabazi (Springer, Cham, 2018), pp. 159–180.
- [18] M. I. Bolotov, L. A. Smirnov, G. V. Osipov, and A. Pikovsky, *JETP Lett.* **106**, 393 (2017).
- [19] M. Bolotov, L. Smirnov, G. Osipov, and A. Pikovsky, *Chaos* **28**, 045101 (2018).
- [20] F. P. Kemeth, S. W. Haugland, L. Schmidt, I. G. Kevrekidis, and K. Krischer, *Chaos* **26**, 094815 (2016).
- [21] Y. Suda and K. Okuda, *Phys. Rev. E* **97**, 042212 (2018).
- [22] O. E. Omel'chenko, M. Wolfrum, and E. Knobloch, *SIAM J. Appl. Dyn. Syst.* **17**, 97 (2018).
- [23] V. Semenov, A. Zakharova, Y. Maistrenko, and E. Schöll, *Europhys. Lett.* **115**, 10005 (2016).
- [24] J. Sawicki, I. Omelchenko, A. Zakharova, and E. Schöll, *Phys. Rev. E* **98**, 062224 (2018).
- [25] W. H. Press, S. A. Teukolsky, W. T. Vetterling, and B. P. Flannery, *Numerical Recipes: The Art of Scientific Computing*, 3rd ed. (Cambridge University Press, New York, 2007).
- [26] X. Zhang, A. Pikovsky, and Z. Liu, *Sci. Rep.* **7**, 2104 (2017).
- [27] C. R. Laing, *SIAM J. Appl. Dyn. Syst.* **16**, 974 (2017).